



## RESEARCH ARTICLE

10.1029/2021JD035019

## Riehl and Malkus Revisited: The Role of Cloud Radiative Effects

Michael R. Needham<sup>1</sup>  and David A. Randall<sup>1</sup><sup>1</sup>Department of Atmospheric Science, Colorado State University, Fort Collins, CO, USA

## Key Points:

- Cloud-longwave feedbacks discussed in previous studies may be examples of a general feedback driven by atmospheric cloud radiative effects
- Warm, humid regions export energy and import moisture in a way similar to the intertropical convergence zone
- The atmospheric cloud radiative effect as a function of column relative humidity is nearly independent of the sea surface temperature

## Correspondence to:

M. R. Needham,  
[m.needham@colostate.edu](mailto:m.needham@colostate.edu)

## Citation:

Needham, M. R., & Randall, D. A. (2021). Riehl and Malkus revisited: The role of cloud radiative effects. *Journal of Geophysical Research: Atmospheres*, 126, e2021JD035019. <https://doi.org/10.1029/2021JD035019>Received 6 APR 2021  
Accepted 15 JUL 2021

**Abstract** The intertropical convergence zone (ITCZ) exports energy and imports moisture. This has been understood for decades. By analyzing a set of uniform, nonrotating aquaplanet simulations, we show that energy export and moisture convergence are general characteristics of warm humid regions, and not just of the ITCZ. Using an analysis method based on the column relative humidity, we find that the absorption of longwave radiation by clouds supplies the energy that is exported from humid regions. The longwave absorption also induces a thermally direct circulation that lifts water vapor and converges moisture into regions that are already quite humid. An additional set of simulations shows that strong atmospheric energy convergence is absent when radiation is homogenized across the domain.

## 1. Introduction

The top of atmosphere (TOA) radiation distribution shows that the tropics are a source of energy for the rest of the planet. Our understanding of tropical energy export is due in large part to the pioneering work of Riehl and Malkus (1958, hereafter RM58). They performed an energy and moisture budget analysis of the Intertropical Convergence Zone (ITCZ, which they called the equatorial trough zone), a narrow belt of moisture convergence and enhanced precipitation that sits a few degrees north of the equator on average (Byrne et al., 2018). Using radiosonde observations from a few dozen sites in the tropics, as well as estimates of the zonal-mean radiative imbalance of the northern hemisphere as a function of the seasons, RM58 showed a net export of energy out of the ITCZ, and a net import of moisture into the ITCZ. The net energy outflow implies an energy source within the ITCZ. The energy transport is accomplished through the upper-level export of dry static energy ( $s$ , the combination of potential energy and dry enthalpy), while the moisture transport is accomplished by the low-level import of water vapor.

RM58 understood that the low-level moisture import and upper-level energy export implies an upward flux of energy within the ITCZ. They considered several possible mechanisms that could accomplish this; diffusion, ascent within synoptic disturbances, or ascent within protected convective updrafts. RM58 observed the now familiar tropical profile of moist static energy ( $h$ , the combination of  $s$  and latent energy) which is uniform with height through the boundary layer, decreases with height above the boundary layer and then increases with height above a mid-tropospheric minimum due to the increase of potential energy. The existence of the minimum led RM58 to eliminate the first two mechanisms: diffusion would be unable to transport energy upward above the minimum because that would go against the energy gradient, and large-scale ascent would eliminate the minimum itself because  $h$  is conserved following an air parcel. RM58 concluded that convective updrafts could “tunnel” through the mid-tropospheric minimum to transport energy from the moist boundary layer to upper levels, where it could then be transported poleward by the Hadley cells. In short, RM58 concluded first that the ITCZ is a source of energy and a sink for moisture due to the export of energy and the import of water vapor, and second that convective-scale ascent is key to the necessary vertical energy transport.

Neelin and Held (1987) analyzed the ITCZ in a manner similar to RM58. They defined a quantity called the Gross Moist Stability (discussed extensively by Raymond et al., 2009) to describe how low-level tropical mass convergence must, on-average, occur in locations where the atmosphere is gaining energy. A net source of energy for an atmospheric column drives low-level moisture convergence into the column, as discussed by RM58. The atmospheric energy source could plausibly come from the surface flux of moist static energy, or the convergence across the column of longwave and shortwave radiation.

© 2021. The Authors.  
This is an open access article under the terms of the [Creative Commons Attribution](https://creativecommons.org/licenses/by/4.0/) License, which permits use, distribution and reproduction in any medium, provided the original work is properly cited.

A large body of work has explored the interactions between clouds and radiation with the use of the cloud radiative effect (CRE, Harrison et al., 1990; Ramanathan, 1987; Ramanathan et al., 1989), defined as the difference between full-sky and clear-sky radiative fluxes. Here, we are particularly interested in the absorption of radiation by clouds. Termed the atmospheric cloud radiative effect (ACRE), this absorption has been shown to greatly impact large-scale phenomena such as the ITCZ and the Hadley cells (Randall et al., 1989; Slingo & Slingo, 1988). Sherwood et al. (1994) investigated the influence of the ACRE on tropical circulations in an atmospheric global circulation model. They found that removing the ACRE above 600 hPa led to a reduction in the strength of the Hadley and Walker circulations. Similar results have been obtained in more recent studies utilizing updated GCMs, which have also noted the role of ACRE in determining the width of the ITCZ, reducing the double-ITCZ bias, and strengthening the precipitation associated with various tropical phenomena (Albern et al., 2018; Benedict et al., 2020; Harrop & Hartmann, 2016; Li et al., 2015; Medeiros et al., 2021; Popp & Silvers, 2017; Voigt & Albern, 2019). For a recent review of the interactions between clouds, radiation, and atmospheric circulations, see Voigt et al. (2021).

Sherwood et al. (1994) also described a positive feedback between ACRE and cloudiness, in which cloud radiative heating drives rising motion, which favors further cloud formation and additional radiative heating. This type of tropical cloud-longwave feedback has recently received a lot of attention in several different contexts. Wing and Emanuel (2014) introduced a new method for investigating the feedbacks that govern convective self-aggregation using the spatial variance of the frozen moist static energy. They found that the longwave flux convergence is strongly positive in extremely humid regions of a cloud resolving model without rotation, and produces a strong positive feedback that maintains an aggregated state. In simulations of rotating radiative-convective equilibrium (Arnold & Randall, 2015; Khairoutdinov & Emanuel, 2018), a similar variance analysis shows the important role of cloud-longwave feedbacks in maintaining a disturbance that resembles the Madden-Julian Oscillation (MJO). Recently, Benedict et al. (2020) used a set of mechanism-denial experiments to show that removing the ACRE weakens the MJO. Medeiros et al. (2021) also found that removing cloud radiative feedbacks weakens tropical precipitation by reducing the frequency of extreme precipitation events. Ruppert et al. (2020) have shown that a similar feedback promotes the intensification of tropical cyclones.

Tropical convective phenomena are strongly coupled to precipitation, which in turn is strongly coupled to humidity (Raymond, 2000). Bretherton et al. (2004) showed that the mean tropical precipitation rate can be described as a simple exponential function of the column relative humidity (CRH, the ratio of the actual to the saturation water vapor path, alternatively known as the saturation fraction). This has been well supported by later studies (Powell, 2019; Raymond & Zeng, 2005; Raymond et al., 2009; Rushley et al., 2018; Wolding et al., 2020). Analysis suggests that this relationship can be understood in terms of the concurrent evolution of precipitation and humidity, in which grid cells slowly build up water vapor to some critical value, at which point they quickly lose water vapor to precipitation (Inoue & Back, 2015; Masunaga & L'Ecuyer, 2014; Neelin et al., 2009; Peters & Neelin, 2006; Wolding et al., 2020).

In a recent paper, Needham and Randall (2021) demonstrated a nonlinear relationship between the mean ACRE and the CRH that is similar to the aforementioned relationship between precipitation and CRH. They also suggested that the ACRE favors the exponential relationship between precipitation and CRH because it facilitates a shift from convective-scale to stratiform ascent (Ahmed & Schumacher, 2015; Jenney et al., 2020).

In this study, we emulate the analysis of RM58 using a set of idealized aquaplanet simulations performed in the absence of rotation with uniform sea surface temperatures (SSTs). We find that the main conclusions of RM58 hold in our idealized simulations even though they do not contain an ITCZ or any other regions with a time-mean convergence of moisture. This suggests that all humid regions of the tropics may function like the ITCZ, in that they export energy and import moisture. Furthermore, we observe a cloud-longwave feedback that is driven by the ACRE in humid regions. This feedback strongly resembles those emphasized in previous studies, as discussed above.

Section 2 provides an overview of the simulations used in this study, and includes a discussion of our analysis methods. In Section 3, we show that the ACRE becomes large in humid regions, consistent with the main conclusions of Needham and Randall (2021). The moisture and energy budgets are analyzed in

Section 4, and the vertical structure is investigated in Section 5. In Section 6, we analyze an additional set of experiments in which radiation is homogenized over the domain. Conclusions are presented in Section 7.

## 2. Data and Methods

### 2.1. Model Simulations

The model output used in this study comes from a set of simulations performed with a super-parameterized version of the Community Atmosphere Model 4 (CAM4), and are the same simulations analyzed in a recent paper by Jenney et al. (2020), where they are described in detail. The model uses a  $0.9^\circ \times 1.25^\circ$  horizontal grid with 26 levels, and covers the entire globe. The three simulations were performed following the protocol of the Radiative-Convective Equilibrium Model Intercomparison Project (hereafter RCEMIP, Wing et al., 2018), and were discussed by Wing et al. (2020). The RCEMIP simulations were performed without rotation and without land. Insolation was held uniform in time and space, and each of the three simulations had a fixed SST of 295 K, 300 K, or 305 K. Our results are based on an analysis of 30 days of hourly mean data from the fourth simulated year in each simulation. We focus on the 300 K simulation, but nearly identical conclusions were reached when the analysis was repeated for the other two simulations. An additional set of experiments was performed to investigate the effect of globally averaged radiation, and are discussed further in Section 6.

The superparameterized version of CAM4 replaces the conventional convection parameterization of the CAM with a two-dimensional cloud resolving model (the System for Atmospheric Modeling, described in Khairoutdinov & Randall, 2003) embedded within each GCM grid column. The CRM uses a horizontal grid spacing of 4 km, with 32 columns. Its 24 CRM levels are aligned with the lowest 24 levels of the GCM. The CRM explicitly simulates convective-scale dynamics, and parameterizes cloud microphysics, radiation, and other processes on its fine grid. Heating and drying rates are averaged across the CRM and are passed back to the GCM. A more detailed discussion of superparameterization is provided by Randall et al. (2016).

### 2.2. Analysis Using the CRH

The RCEMIP simulations omit the Coriolis effect and meridional temperature gradient which give rise to an ITCZ in the real tropics and in more realistic simulations. These uniform conditions prevent the formation of regions characterized by a time mean convergence of moisture. However, this does not mean that water vapor is uniform. Instead, at any given moment the RCEMIP simulations contain a few large, heavily precipitating regions which slowly migrate within a broader dry environment. Snapshots showing the OLR, precipitable water, and 500 hPa vertical velocity for the 300 K simulation are shown in Figure 1.

To investigate how the dry and humid regions interact, we analyze the three RCEMIP simulations using the CRH,

$$\text{CRH} = 100\% \times \frac{\int_{p_t}^{p_s} q dp}{\int_{p_t}^{p_s} q^*(T) dp}. \quad (1)$$

Model diagnostics are analyzed by taking the area-weighted average value of a field using only those grid cells with CRH within a bin of width 2%, and then repeating for all bins between 0% and 100% CRH. Similar analyses using the CRH have been used previously (e.g., Bretherton et al., 2005; Jenney et al., 2020; Wing & Emanuel, 2014), and the method used here is identical to that of Needham and Randall (2021).

The curves in Figure 2 show the probability density function (PDF) of the CRH for each of the three RCEMIP simulations, with the curve for the 300 K simulation emphasized using a heavy black line. Each of the simulations has a peak in the CRH distribution between 60% and 75%. As the SST increases, the PDFs become wider and shorter, which indicates more extremely dry and extremely humid grid cells in the 305 K simulation compared to the 295 K simulation. Each of the PDFs goes to zero near 20% and 90%. Summary statistics for the CRH are included in Table 1.

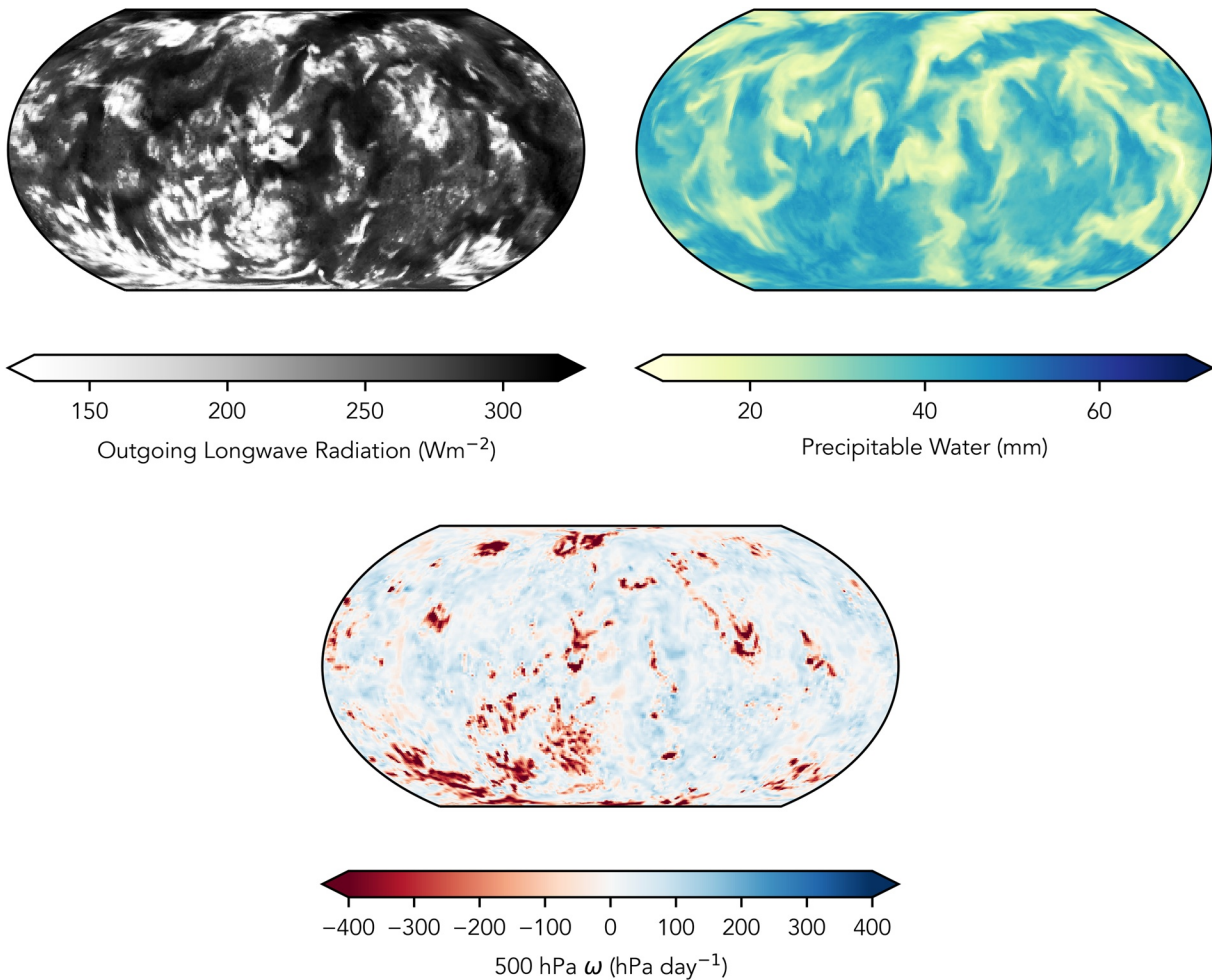


**Figure 1.** Outgoing longwave radiation (top left) precipitable water (top right), and vertical velocity across the 500 hPa surface (bottom), at the same arbitrary time step for the 300 K simulation.

### 3. CRE Versus CRH

The CRH binning method was used to calculate the mean vertically integrated full-sky and clear-sky radiative heating rates for each of the three RCEMIP simulations, which are shown in the top row of Figure 3. The full-sky rate (thick lines) is the total heating rate due to radiation, while the clear-sky rate (thin lines) is the heating rate that would occur if clouds were made invisible to radiation, leaving only the radiative effects of temperature, humidity, aerosols, and any radiatively active gases. Panel (a) illustrates that the longwave heating rates are negative in both dry (low CRH) and humid (high CRH) regions. As the CRH increases, the increase in water vapor leads to more radiative cooling of up to about 60%, at which point the cooling rate begins to strongly decrease with further increases of the CRH due to the presence of clouds. This decrease does not occur in the same way for the clear-sky rate so that the ACRE, calculated as the full-sky minus the clear sky rates (and shown in panel d) begins to increase dramatically in humid regions. As the SST increases from 295 K to 300 K and 305 K, both the full-sky and clear-sky cooling increase in magnitude. However, these increases occur at roughly the same rate, so that the ACRE remains unchanged.

The shortwave heating rates are shown in panel (b), and increase only slightly as the CRH increases, compared to the longwave. The full-sky and clear-sky rates are very close together, indicating that clouds do not account for a large amount of shortwave absorption. Consequently, the shortwave ACRE (panel e) is nearly zero in dry regions, and is small in humid regions compared to the longwave effect. Together, the net ACRE is largely determined by the longwave effect, consistent with the previous work (Allan, 2011; Slings &

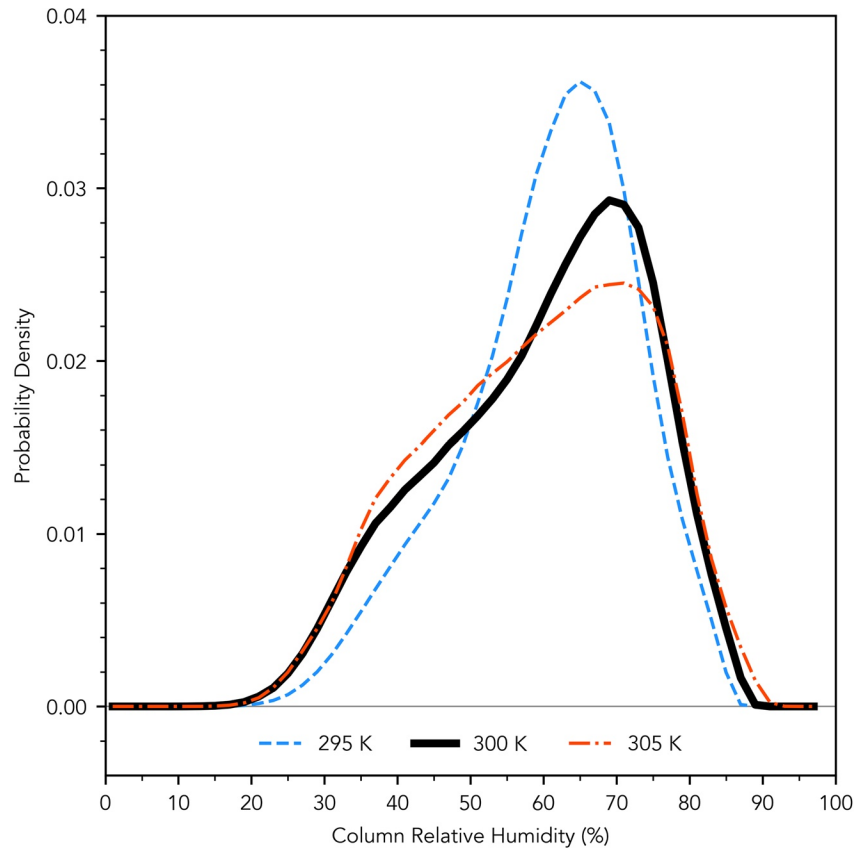


**Figure 2.** Probability density function of column relative humidity for each of the three Radiative-Convective Equilibrium Model Intercomparison Project simulations.

Slingo, 1988). This is in contrast to the CRE at the top of the atmosphere, which includes a strong shortwave component (Harrison et al., 1990; Hartmann & Berry, 2017; Ramanathan et al., 1989). The mean longwave ACRE is small in dry regions and begins to increase rapidly as the CRH exceeds a value of about 70%.

A key conclusion of Needham and Randall (2021) was that the mean ACRE for a particular CRH was nearly identical in different regions of the tropics. The same conclusion is reached here in the context of these idealized simulations: as the SST increases, the ACRE at a given CRH appears to be nearly unchanged. Changes to the ACRE in a warmer climate may then be due only to changes in the CRH, although this hypothesis needs further study. Another important conclusion from Figure 3 is that the net radiative heating rate changes sign to become positive in extremely humid regions (panel c). This sign change is central to the discussion in Section 5.

Figure 4 shows the CRE binned by the CRH only for the 300 K simulation. The panels in Figure 4 include the median (solid line) as well as the mean (dotted line), and the shading represents the interquartile range

**Table 1**

Summary Statistics of the CRH for Each of the Simulations, As Well As Domain-Average Values of the TOA CRE and the ACRE

	Mean (%)	$\sigma$ (%)	Skewness	Kurtosis	Mode (%)	CRE ( $\text{W m}^{-2}$ )	ACRE ( $\text{W m}^{-2}$ )
295 K	60.753	11.947	-0.489	-0.176	64.875	-14.142	22.641
300 K	59.910	15.075	-0.446	-0.703	69.375	-18.858	23.766
305 K	59.381	15.127	-0.258	-0.776	70.875	-16.979	26.121

Abbreviations: ACRE, atmospheric cloud radiative effect; CRE, cloud radiative effect; CRH, column relative humidity; TOA, top of atmosphere.

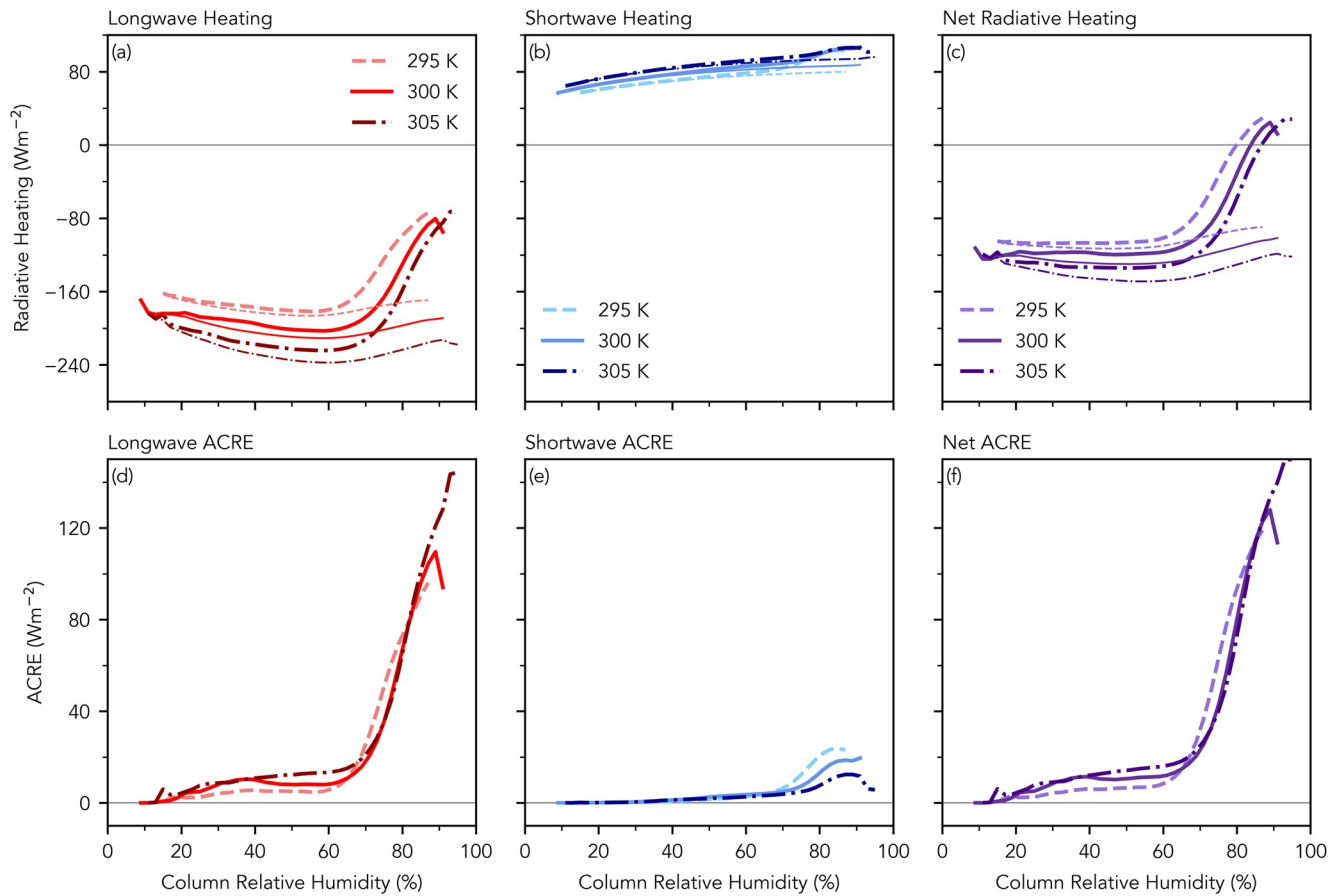


**Figure 3.** Top left: Integrated full-sky (thick lines) and clear sky (thin lines) longwave heating rates for each of the Radiative-Convective Equilibrium Model Intercomparison Project simulations as a function of the column relative humidity. Top middle and top right: Same as top left, but for shortwave and net radiative heating rates. Bottom row: Same as top row, but for the atmospheric cloud radiative effect (ACRE).

within each CRH bin. The top row of the figure shows the longwave, shortwave, and net CRE at the TOA as functions of the CRH. The middle row shows the CRE at the surface, and the bottom row shows the vertically integrated ACRE, calculated as the difference between the two.

The longwave CRE at the TOA (panel a) is small in dry regions but begins to increase as the CRH exceeds a value of about 70%. The shortwave CRE (panel b) behaves qualitatively the same as the longwave effect, but is of larger magnitude and of opposite sign. The negative shortwave effect is larger than the positive longwave effect so the net CRE at the TOA (panel c) is negative in all regions. The CRE reaches its largest magnitude in humid regions, as expected. At the surface, the longwave effect (panel d) is small and positive, due to the enhanced longwave emission from cloud bases. The shortwave effects in panels (b) and (e) are almost identical, which shows that the effect of clouds on shortwave radiation is felt mostly at the surface, rather than in the atmosphere itself, and is due to the enhanced cloud albedo. The net CRE at the surface is, like the TOA effect, largely determined by the shortwave (panel f).

In panel (g) of Figure 4, the longwave ACRE is skewed in dry regions, with the median value near zero while the mean value exceeds the 75<sup>th</sup> percentile. This indicates that in dry regions clouds usually have little to no effect, with the exception of a few clouds which absorb a large amount of longwave radiation. This may be the effect of high cirrus clouds which are advected away from humid regions into dry regions, and trap longwave emission from the surface and lower levels of the atmosphere. In humid regions, the distribution becomes much less skewed as the mean and median are nearly identical. The shortwave ACRE (panel h) reaches its largest magnitude in humid regions, but is still very small compared to the surface shortwave CRE, which again shows that clouds reflect much more sunlight than they absorb. Because the shortwave

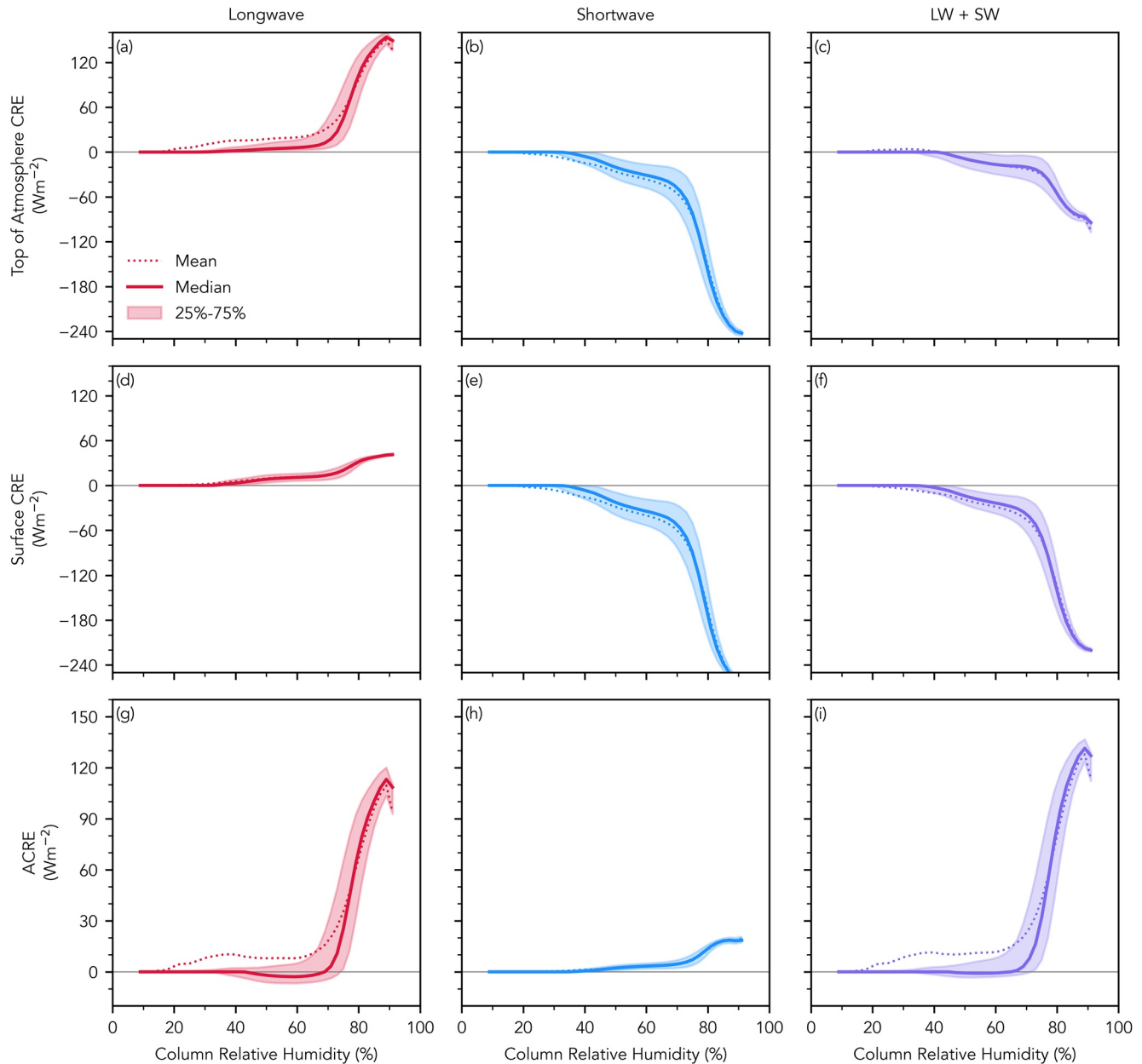


**Figure 4.** (a) Longwave cloud radiative effect at the top of the atmosphere, binned by the column relative humidity (CRH). The dotted line shows the area-weighted average cloud radiative effect (CRE) in each CRH bin, the solid line shows the 50th percentile, and the shading shows the interquartile range. (b and c) Same as (a), but for the shortwave and net CRE. (d–f) Same as (a–c), but for the surface CRE. (g–i) Same as (a–c), but for the atmospheric cloud radiative effect (ACRE). All panels show data from the 300 K simulation. Positive (negative) values indicate net heating (cooling).

effect is so small, the net ACRE (panel i) is dominated by the longwave component, and is characterized by the same skewed distribution in dry regions and rapid strengthening in humid regions. However, the net ACRE is slightly larger than the longwave ACRE due to the positive shortwave contribution.

Figure 4 shows that in extremely humid regions the net CRE at the TOA is dominated by the shortwave effect. At first glance, this may appear to conflict with previous studies which have found that the net TOA CRE nearly cancels in the tropics (Hartmann & Berry, 2017; Ramanathan et al., 1989). However, as seen in Figure 2, only a small number of grid cells have a CRH greater than 80%. When the domain-mean CRE is calculated, these extremely humid grid cells do not carry much weight. This is further illustrated by recognizing that the domain mean of any of the terms in Figure 4 can be calculated as  $\bar{x} = \sum_{CRH} x(CRH) \times PDF(CRH)$ ,

following the method of Bony et al. (2004). In Table 1, the domain-mean CRE does not exceed  $20 \text{ W m}^{-2}$  for any of the three simulations.

When the CRE is decomposed into surface and atmospheric components, the shortwave effect acts primarily at the surface, while the longwave effect determines the ACRE. Panel (i) shows that the net ACRE can be a large heat source for the atmosphere, on the order of  $100 \text{ W m}^{-2}$  in very humid regions. To see the impact of this atmospheric energy convergence, we perform an analysis of the energy and moisture budgets, following the lead of Riehl and Malkus (1958).

#### 4. Budgets of Energy and Moisture

To interpret the following budget analyses, it is important to keep in mind the differences between the RCE-MIP simulations and the real earth, which were mentioned above in Section 2. The RCEMIP simulations are performed without rotation and without meridional SST gradients, and they are forced with spatially uniform insolation. This means that while the temperature and lack of Coriolis acceleration lead to “tropical” conditions, the simulations do not have a true “tropics” in the sense that there are no regions characterized by a time-mean surplus of radiative energy that must be exported to higher latitudes. The absence of rotation also means that there is no ITCZ. More generally, there are no regions that are characterized by a time-mean convergence or divergence of moisture or energy. Needham (2021) obtained similar results for a set of aquaplanet simulations with rotation, a meridional SST gradient, and a diurnal cycle.

We now turn to an analysis of the budgets of energy and moisture in the RCEMIP simulations. The time-mean energy balance of an atmospheric column can be understood in terms of the convergence of energy into that column from the TOA or surface (Chen & Bordoni, 2014), written as

$$\left\langle \frac{\partial h}{\partial t} \right\rangle + \left\langle \mathbf{V} \cdot \nabla h \right\rangle + \left\langle \omega \frac{\partial h}{\partial p} \right\rangle = \overline{F_{\text{net}}}. \quad (2)$$

In Equation 2,  $\langle x \rangle$  represents the mass-weighted vertical integral of a quantity  $x$ ,  $\bar{x}$  represents a temporal mean, and  $h$  is the moist static energy, defined as  $h = s + L_v q$ , where the dry static energy  $s$  is defined as  $s = c_p T + gz$ .  $F_{\text{net}}$  is the net flux of energy into the column, and is given by

$$F_{\text{net}} = (LW + SW)_{\text{toa}} + (LW + SW)_{\text{sfc}} + SH + LE. \quad (3)$$

In words, the time mean atmospheric energy flux convergence  $F_{\text{net}}$  depends on the fluxes of longwave and shortwave radiation across the top of the atmosphere and surface, as well as the surface fluxes of sensible heat (SH) and latent energy (LE).

The terms comprising  $F_{\text{net}}$  for the 300 K simulation are shown in Figure 5, where they have been binned by the CRH similar to Figures 3 and 4. The longwave flux at the TOA and surface is shown as the red dashed line in panels (a) and (b). Both fluxes decrease in magnitude as the CRH increases, but the magnitude of the TOA flux begins to decrease more rapidly when the CRH exceeds about 70%. As discussed in connection with Figures 3 and 4, the change in the longwave convergence is due to the ACRE. The shortwave fluxes are shown as the blue dash-dotted line in the top two panels. Both the TOA and surface shortwave terms show a decrease in magnitude in humid regions. In contrast to the longwave, this does not represent a strong convergence of shortwave radiation, but instead is the result of the enhanced cloud albedo effect which reflects solar radiation back to space. The atmospheric shortwave convergence (panel c) shows little dependence on the CRH. Similarly, the surface flux of moist static energy, shown as the green dotted line in panel (b), does not change much as the CRH increases.

The sum of the longwave, shortwave, and surface heat flux terms is shown as the thick black line in panel (c), which represents the net convergence of energy into the atmosphere as a function of the CRH (i.e.,  $F_{\text{net}}$  in Equation 3). In dry regions,  $F_{\text{net}}$  is near zero or slightly negative, as shortwave heating and surface fluxes are balanced by longwave cooling. In humid regions, the longwave term becomes small while the shortwave and surface heat flux terms do not depend much on the CRH. This leads to an increase in  $F_{\text{net}}$  which corresponds to a strong convergence of energy into the atmosphere. As discussed previously (Figure 3), the

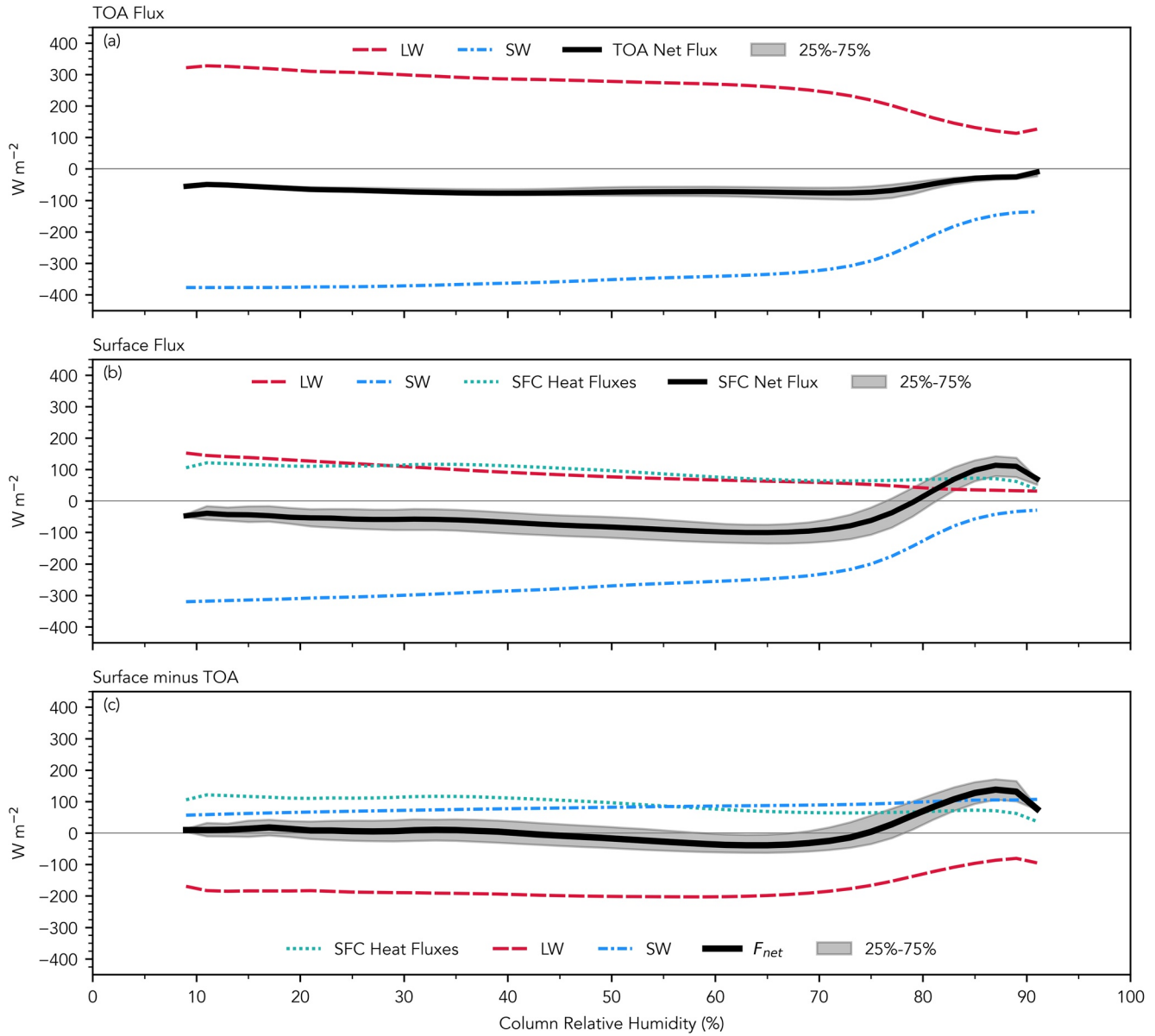


**Figure 5.** Energy budget binned by the column relative humidity at the top of atmosphere (TOA) (a), surface (b), and across the atmosphere (c) In panels (a and b), upward values are positive, while in (c) positive is defined as a net atmospheric heating.

full-sky longwave heating becomes weak in humid regions while the clear-sky heating does not. This indicates that the increase in  $F_{net}$  is due to a strong longwave ACRE.

Because the energy budget was computed over the entire domain, positive  $F_{net}$  in humid regions and negative  $F_{net}$  in dry regions imply an export of energy out of humid regions and into dry regions. Positive  $F_{net}$  also implies low-level horizontal mass convergence into humid regions (Neelin & Held, 1987), which has a strong impact on the moisture balance. The time-mean integrated moisture convergence of the atmosphere is given (again following [Chen & Bordoni, 2014]) by

$$\left\langle \frac{\partial q}{\partial t} \right\rangle + \left\langle \mathbf{V} \cdot \nabla q \right\rangle + \left\langle \omega \frac{\partial q}{\partial p} \right\rangle = \bar{E} - \bar{P} \quad (4)$$

where  $P$  and  $E$  represent the rates of precipitation and evaporation. Time averaging allows us to neglect the time derivative in Equation 4. This leads to a simple water cycle in which the moisture that enters the

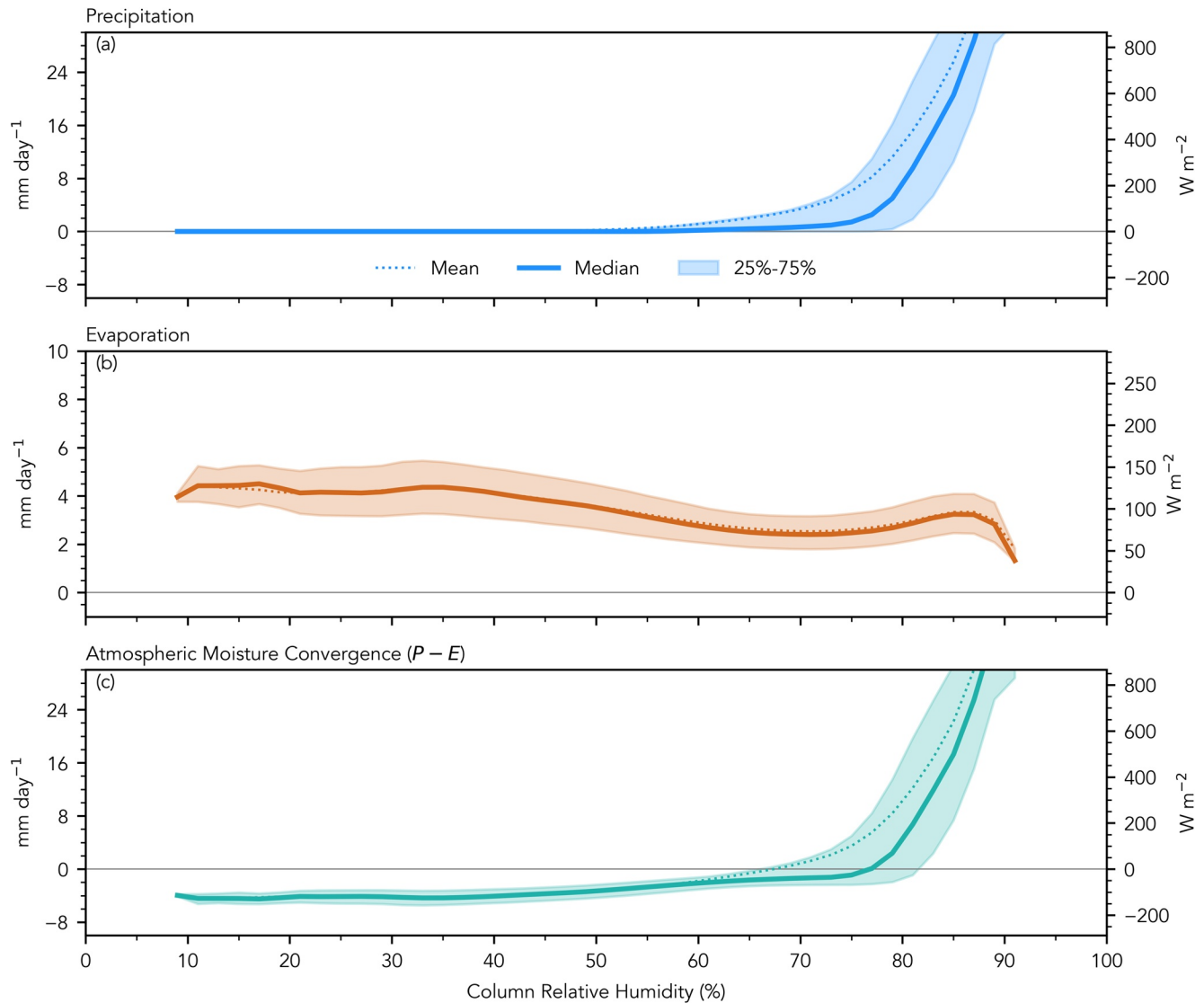


**Figure 6.** As in Figure 5, but for the terms in the atmospheric moisture budget. Note the different scale for panel (b).

atmosphere through surface evaporation, is transported through dynamic processes, and then exits the atmosphere, typically in another location, as precipitation.

The surface moisture budget for the 300 K simulation is shown in Figure 6. Panel (a) shows the mean and median precipitation rate binned by the CRH, as well as the interquartile range. As expected, the precipitation rate depends exponentially on the CRH (Bretherton et al., 2004), and begins to increase rapidly beyond 70%–80%. The separation between the mean (dotted line) and median (dashed line) precipitation shows that the distribution is skewed, with a large number of events with little or no precipitation and a few downpour events. In contrast to the precipitation rate, the evaporation rate (panel b), shows little dependence on the CRH. The mean evaporation rate ranges between 2 and 6 mm day<sup>-1</sup> while the precipitation rate can exceed 50 mm day<sup>-1</sup> in extremely humid regions. This shows that the moisture convergence calculated from Equation 4 supplies the precipitation.

The budgets of energy and moisture allow us to draw two general conclusions about humid tropical regions. First, humid regions are characterized by a strong longwave ACRE which leads to a net convergence of energy into the atmosphere. This then implies a horizontal transport of energy within the atmosphere from humid to dry regions. Second, humid regions are characterized by vertically integrated moisture convergence

against the moisture gradient, which then leads to enhanced precipitation. We emphasize again that the energy export and moisture import in humid regions are not the result of rotation or SST gradients, which are not included in the RCEMIP simulations. Instead they are a general characteristic of warm humid regions. Our conclusions mirror those of RM58, who found that the ITCZ is a region of intense energy export as well as up-gradient moisture transport. RM58 presented their work at a time when the importance of radiative heating was not fully appreciated. They speculated that the energy export out of the ITCZ might be fueled by surface energy fluxes. Our results (Figure 5) suggest that instead the ACRE serves as the primary heat source. The importance of radiative heating to the transports of moisture and energy is discussed further in Section 6.

In addition to demonstrating that the ITCZ is a sink of moisture and a source of energy for the rest of the atmosphere, RM58 also realized this implied a vertical energy transport within the ITCZ to balance the energy export. They noted that the mid-tropospheric minimum in moist static energy is not consistent with large-scale vertical energy transport. They instead proposed that convection provided the necessary transport because deep convective updrafts could lift energy to the upper levels of the atmosphere and bypass the moist static energy minimum. Recent work by Jenney et al. (2020) used a CRH analysis method similar to the one used in this study to show a shift to large-scale ascent, including environmental ascent, in extremely humid regions of these same RCEMIP simulations. In the following section, we explore the implications of large-scale ascent in humid regions, and its effects on the vertical transports of moisture and energy.

## 5. Moistening of the Troposphere Through Environmental Ascent

### 5.1. The Vertical Distribution of Static Energies

The transports of energy in the atmosphere can be understood using the dry and moist static energies, which were defined in Section 4. Both  $h$  and  $s$  are approximately conserved under dry adiabatic processes. In addition,  $h$  is approximately conserved under condensation or evaporation.

The top row of Figure 7 shows contours of  $h$  as a function of altitude and CRH, with similar contours for  $s$  and latent energy. The contours were found by calculating the area-weighted profile of a field for each CRH bin of width 2%. This allows for the comparison of the vertical structure of the terms that make up  $h$  between dry and humid regions.

The contours in panel (a) show the typical distribution of  $h$  in the tropics. The most obvious feature is the mid-tropospheric minimum (marked by the black contour) which was emphasized by RM58. The altitude where the minimum occurs depends on the CRH; it is near 2 km in dry regions, rises to 5 km at 70% CRH, then drops back to 2 km in extremely humid regions. In addition, the minimum becomes less distinct in humid regions. This can be seen in panel (d), which shows contours of the vertical gradient of  $h$ . In dry regions, the minimum is distinct, with large values of the gradient above and below the black contour. However in humid regions, the vertical gradient becomes weaker, especially above the minimum. As will be discussed later, this has important implications for the vertical transport for  $h$ .

The dry static energy (panel b) is largely independent of the CRH. This is to be expected, as the lack of rotation in the RCEMIP simulations means that horizontal gradients of temperature are swiftly removed (Charney, 1963; Sobel et al., 2001). In contrast, panel (c) shows that the distribution of latent energy is strongly tied to the CRH. In dry regions, water vapor is largely relegated to lower levels, but in humid regions, water vapor extends through a much deeper layer of the troposphere. Comparison of panels (b) and (c) illustrates that the change in both the magnitude and altitude of the minimum are due to changes in latent energy rather than dry static energy. In fact, the weakening of the minimum in  $h$  appears to be the result of a large quantity of water vapor above the black contour, which also acts to reduce the vertical gradient.

The lifting of water vapor is a natural consequence of the shift to environmental ascent in humid regions, as discussed by Jenney et al. (2020), and illustrated in panels (e) and (f), which show the mass flux on convective and large scales. In panel (e), “intense” refers to the CRM mass flux, which is by default calculated only when the CRM vertical velocity exceeds  $2 \text{ m s}^{-1}$  in a 4-km wide CRM grid column. In panel (f), “large-scale” refers to the mass flux computed using the GCM vertical velocity which includes contributions from the CRM as well as from the environment. The environmental mass flux can be calculated as the difference

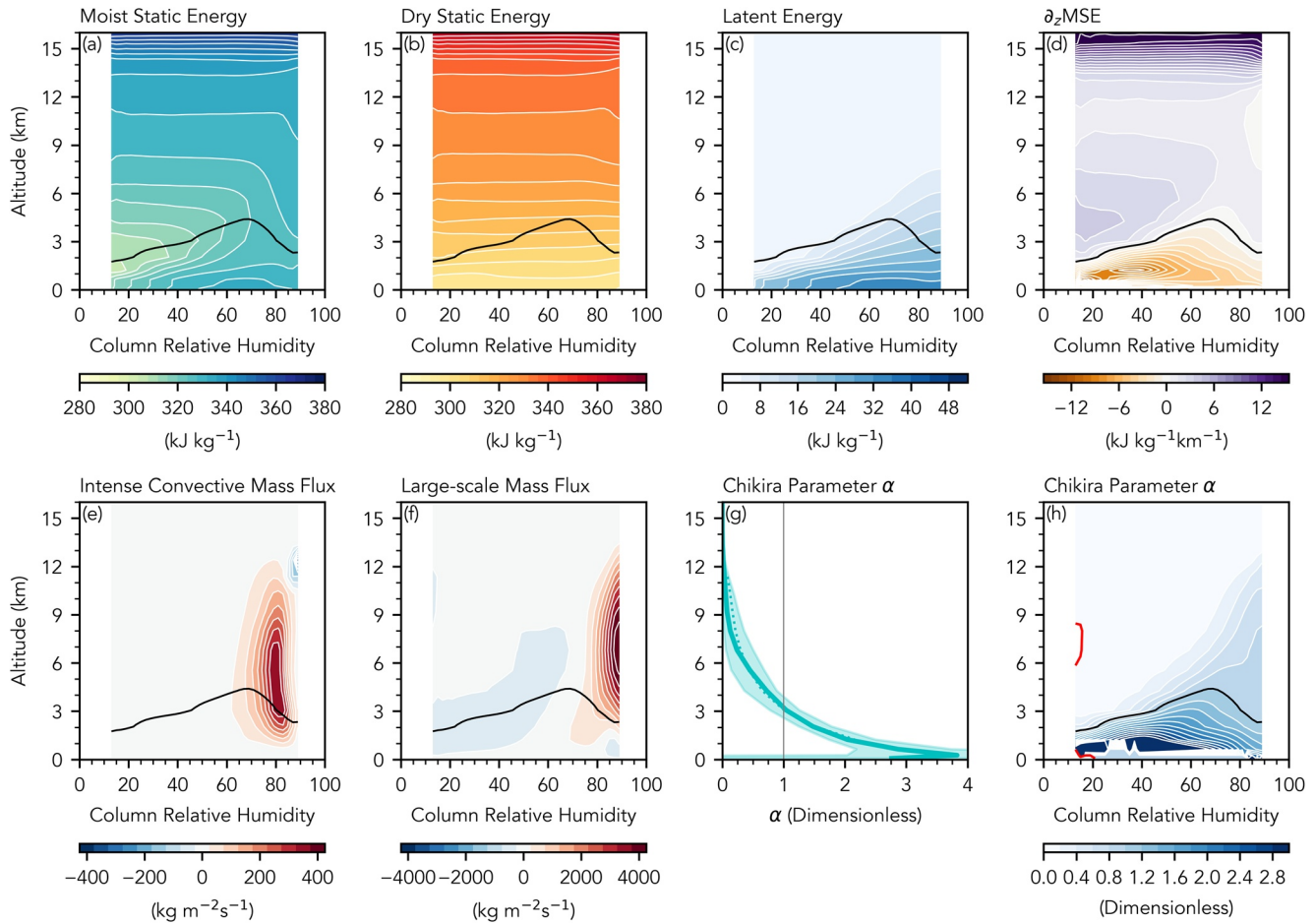


**Figure 7.** (a) Profiles of moist static energy binned by the column relative humidity. (b–f and h) Same as (a), but for the dry static energy, the latent energy, the vertical moist static energy gradient, the convective-scale mass flux, the large-scale mass flux, and the Chikira parameter ( $\alpha$ ), respectively. In all panels except for (g), the thick black line shows the level of the moist static energy minimum. In panel (h), the black contour also represents the level where  $\alpha = 1$ , and the red contour marks the level where  $\alpha = 0$ . Panel (g) Domain-average profile of  $\alpha$  with the interquartile range shaded.

between large-scale and convective (i.e., GCM and CRM) mass fluxes. The environmental flux is omitted from Figure 7 because it is very similar to the large-scale flux when plotted against CRH and height.

The intense convective mass flux maximizes near 80% CRH, but rapidly decreases in magnitude as the CRH continues to increase. In contrast, the large-scale mass flux shows weak descent through much of the domain and only becomes positive in the middle troposphere when the CRH exceeds 75%. As the CRH continues to increase, the large-scale mass flux also increases in magnitude, reaching its largest value near 90%, the highest CRH value observed in the simulation. Importantly, in extremely humid regions, the large-scale mass flux is an order of magnitude larger than the intense convective mass flux. Then, the large-scale ascent is not determined by strong convection, which weakens in extremely humid regions, but is instead due to the ascent of the environment around any convective updrafts.

## 5.2. Environmental Ascent in Humid Regions

What causes this environmental ascent that lifts water vapor in the troposphere? Ascent on convective scales is a buoyancy-driven process while environmental ascent is driven by sources of heating on larger scales. Evidently there must be some heating in humid regions that drives the environmental ascent implied by panels (e and f) of Figure 7.

Our investigation of the possible sources of heating and moistening in humid regions follows the work of Chikira (2014), who linked the moisture tendency to environmental ascent outside of cumulus updrafts. Chikira (2014) used the weak temperature gradient approximation (Charney, 1963; Sobel et al., 2001) to derive a form of the specific humidity equation that relates the large-scale moisture tendency to various sources of heating,

$$\frac{\partial q}{\partial t} = (\alpha - 1)(C - E) + \frac{\alpha}{L_v}(Q_r + Q_a) + S_0. \quad (5)$$

We have include a simplified form of the equation here, and refer the interested reader to Chikira's paper for the derivation of the full equation. In Equation 5,  $C - E$  refers to the net rate of condensation minus re-evaporation.  $Q_r$  represents the heating due to radiation, and  $Q_a$  represents the heating due to other terms such as liquid-ice phase changes and vertical diffusion.  $S_0$  collects several additional terms due to detrainment, subgrid scale diffusion, and high-frequency waves.

The first two terms on the RHS of Equation 5 are each multiplied by a parameter  $\alpha$ , which is defined equivalently as

$$\alpha \equiv -\frac{L_v}{c_p \pi} \left( \frac{\partial q}{\partial z} \right) \left( \frac{\partial \theta}{\partial z} \right)^{-1} = -L_v \left( \frac{\partial q}{\partial z} \right) \left( \frac{\partial s}{\partial z} \right)^{-1} = 1 - \left( \frac{\partial h}{\partial z} \right) \left( \frac{\partial s}{\partial z} \right)^{-1}, \quad (6)$$

where  $\pi$  is the exner function. The parameter  $\alpha$  determines the moisture tendency due to a particular source of heating. The mechanism for this moistening is straightforward: a localized heating induces environmental rising motion. If the vertical moisture gradient (included in the definition of  $\alpha$ ) is large enough, the environmental ascent will lead to a net upward transport of water vapor. For the  $Q$  terms, any positive heating will tend to moisten the environment if  $\alpha$  is positive. However,  $C - E$  can only moisten the environment if  $\alpha$  exceeds one. Then, the vertical distribution of  $\alpha$  determines whether a particular source of heating can account for the water vapor lifting discussed previously.

If the environmental conditions are known, specifically the vertical moisture gradient (and by extension,  $\alpha$ ), then Equation 5 quantifies the moisture tendency of each heat source. This gives a method for decomposing the total moisture tendency associated with different processes. Similar equations have been used in recent studies to investigate how different sources of heating contribute to the total vertical advection of moisture within the MJO (Chikira, 2014; Janiga & Zhang, 2016; Wolding & Maloney, 2015; Wolding et al., 2016, 2017).

The domain-average profile of  $\alpha$  is shown in panel (g) of Figure 7. Consistent with Chikira (2014),  $\alpha$  is greater than one in the lower troposphere. This means that any net heating will tend to moisten the atmosphere by inducing rising motion: including heating from condensation. Above the level where  $\alpha$  passes through one, heating from condensation can no longer moisten as the conversion to condensed water dominates over any moistening due to rising motion. However, moistening above this level can occur due to other processes, including radiative heating.

The contours in panel (h) of Figure 7 show the vertical structure of  $\alpha$  in dry and humid regions. As with the domain-average profile,  $\alpha$  is greater than one in the lower troposphere in all regions. However there are several differences in the distribution of  $\alpha$  between dry and humid regions. First, the  $\alpha = 1$  contour does not occur at a fixed altitude, but varies between 2 and 5 km because it corresponds exactly to the altitude of the minimum of  $h$ , as can be inferred from Equation 6. This indicates that heating due to condensation cannot account for the vertical moisture transport above the minimum of  $h$  that is implied from the distribution of water vapor in panel (c) of Figure 7. Above the minimum, some heat source other than condensation is required, with radiation as a likely possibility. Typically, radiation does not heat the troposphere, as the longwave emission from water vapor leads to a net radiative cooling. However as seen in panel (c) of Figure 3, the integrated net heating rate becomes positive in humid regions, due to a strong longwave ACRE.

The radiative tendency profiles binned by the CRH are shown in the top row of Figure 8. In dry regions, the longwave tendency (panel a) is concentrated below 2 km, where the moist boundary layer favors radiative cooling from water vapor. As the CRH increases, the distribution of water vapor becomes deeper (shown above in Figure 7c) and the maximum in the longwave temperature tendency shifts to higher altitudes. This

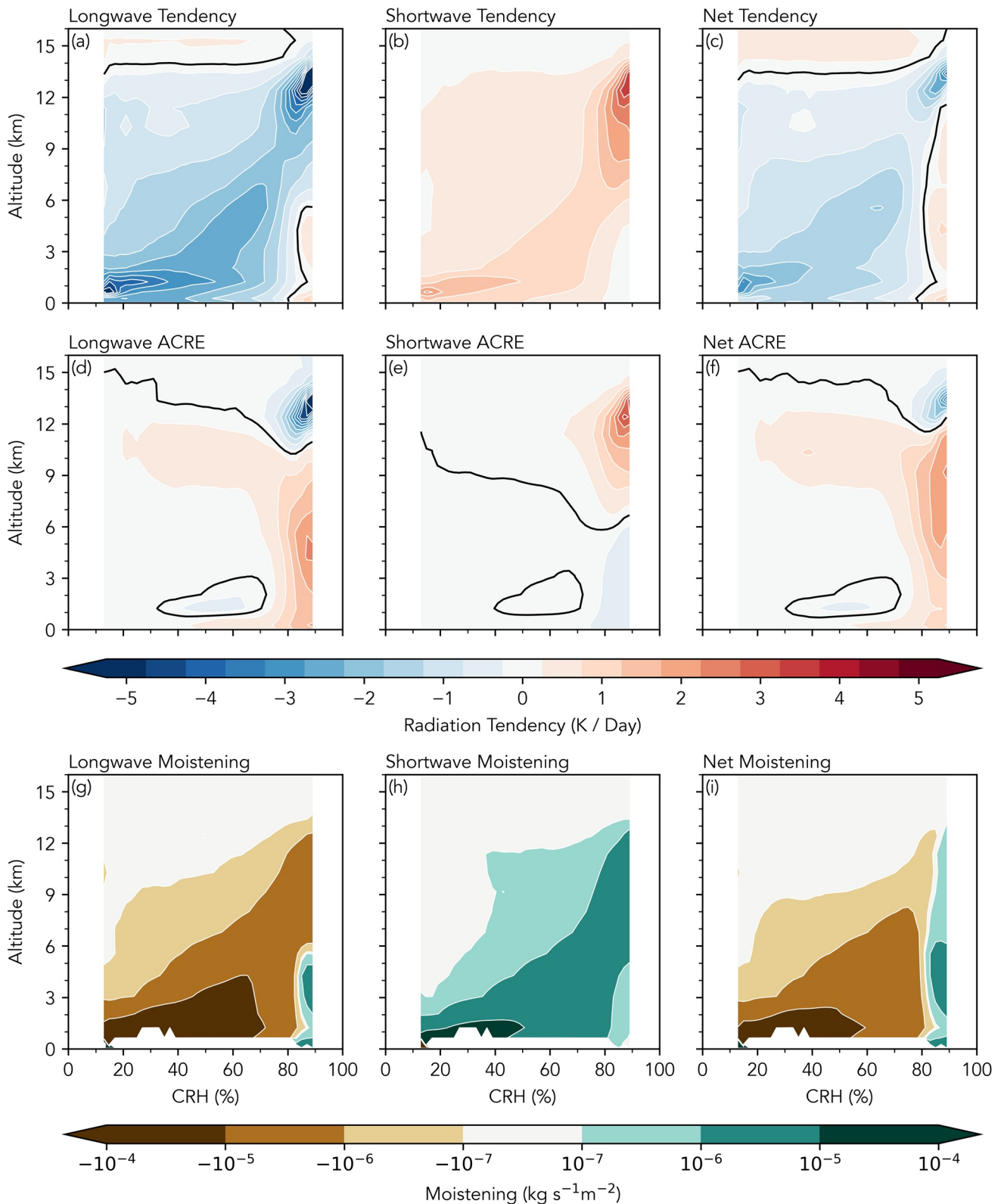


**Figure 8.** (a) Vertically resolved longwave radiation tendency, binned by column relative humidity (CRH). (b and c) Same as (a), but for the shortwave and net radiation tendencies. (d–f) Same as (a–c), but for the atmospheric cloud radiative effect (ACRE). In (a–f), the solid black line shows the zero contour. (g) Moisture tendency due to longwave radiation, defined in the text. (h and i) Same as (g), but for the moistening due to shortwave and net radiation. Note the logarithmic color scale for panels (g–i).

leads to a top-heavy longwave profile in humid regions, characterized by emission from the tops of clouds. This profile is also characterized by a reduction in longwave cooling in the lower troposphere. In extremely humid regions of the lower troposphere the longwave tendency changes sign to become positive.

The shortwave profile (panel b) is everywhere positive and mimics the longwave profile, shifting from a lower-level maximum in dry regions to an upper-level maximum in humid regions. When the longwave and shortwave tendencies are combined (panel c), the net profile is largely determined by the stronger longwave component and tends to cool the atmosphere. The crucial exception is in humid regions, where the weak longwave heating below combined with shortwave heating aloft leads to a deep layer with a net positive radiation tendency.

The vertically integrated heating rates shown in Figure 3 suggest that this heating is due to the ACRE rather than to clear-sky effects (i.e., it is not the result of changes to the distribution of water vapor). This is further supported by the vertically resolved ACRE, shown in the middle row of Figure 8. The longwave ACRE in panel (d) shows a strong heating through most of the troposphere in humid regions up to the level of cloud-top cooling. The shortwave ACRE (panel e) is strongly positive aloft in humid regions due to enhanced absorption of solar radiation by clouds, which leads to a slightly negative shortwave ACRE in lower levels of humid regions. The sum of the longwave and shortwave ACRE is positive through most of the troposphere in humid regions, and its structure is determined largely by the longwave contribution. This positive ACRE is strong enough to change the sign of the radiation tendency and leads to a net radiative heating in humid regions, as seen in panel (c).

To see how this net heating impacts the vertical advection of water vapor, the moistening of the troposphere due to radiation can be written using Equation 5 as

$$\left(\frac{\partial q}{\partial t}\right)_r = \frac{\alpha}{L_v}(Q_{rl} + Q_{rs}). \quad (7)$$

In Equation 7,  $Q_{rl}$  and  $Q_{rs}$  represent the longwave and shortwave heating rates in  $\text{W m}^{-2}$  (i.e., not the radiative tendencies in  $\text{K s}^{-1}$ ). The bottom row of Figure 8 shows the longwave, shortwave, and net moistening of the troposphere due to radiation, calculated using Equation 7 and then binned by the CRH to give contours. As  $\alpha$  is almost universally positive, the sign of the moisture tendency is determined entirely by the sign of the radiation terms. Because of this, radiation largely dries the atmosphere due to cooling-induced subsidence, but in humid regions, the net radiative heating-induced ascent moistens a deep layer of the troposphere in regions that are already quite humid. This suggests that in addition to the transports of energy and moisture between humid and dry regions, radiation plays an important role in the vertical transport of energy and moisture within humid regions. Radiation cools the environment in clear regions, but in extremely humid regions with large amounts of stratiform cloudiness, the powerful ACRE leads to a net radiative heating which induces environmental ascent.

## 6. Additional Simulations With Homogenized Radiation

Thus far, we have shown that humid regions import moisture and export energy, and have suggested that radiative effects play a central role in these processes. In particular, we have shown that the net radiative heating rate in humid regions becomes positive, which leads to large-scale rising motion and additional moisture convergence. To better understand the role of radiation in this process, we now analyze an additional simulation in which the combined radiative heating rate ( $Q_{rl} + Q_{rs}$ ) has been homogenized at each level on each time step. Our method follows studies that have investigated the mechanisms controlling the self-aggregation of convection in RCE simulations (see Wing et al., 2017, and references therein).

Two non-rotating aquaplanet simulations were performed using the standard (without SP) version of CAM4 with the same grid resolution as the previous simulations. The setup for the first simulation (hereafter “Control”) followed the experimental protocol for RCEMIP with a fixed SST of 300 K. The second simulation (hereafter “RadAvg”), was identical to the Control simulation with the exception of the radiative temperature tendency. First, the longwave and shortwave temperature tendencies were calculated for each column and level as in the Control case. Then, the global mean temperature tendency was found, and this

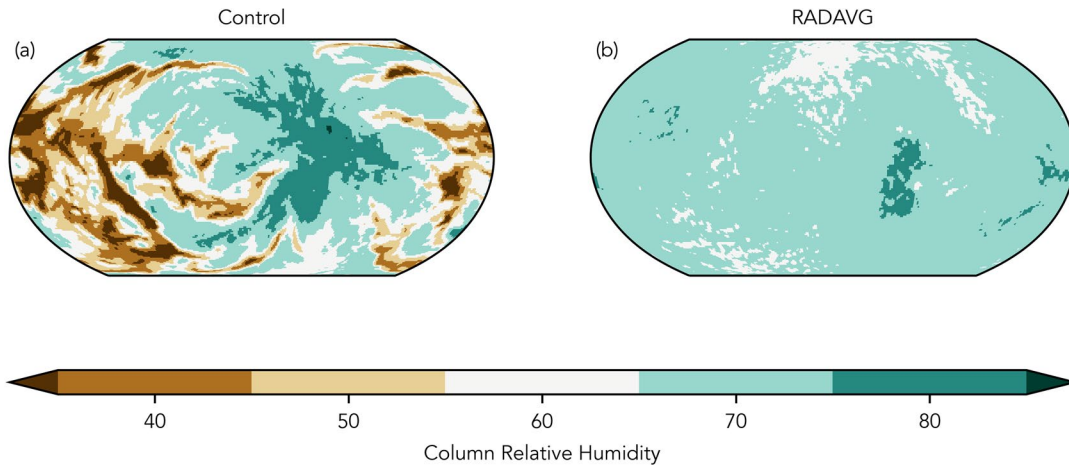


**Figure 9.** Snapshot of daily mean column relative humidity at an arbitrary time step for the Control (a) and RadAvg (b) simulations.

average value was used to update the GCM temperature for each column. This process homogenizes CREs, and removes impacts that arise due to inhomogeneous radiative heating.

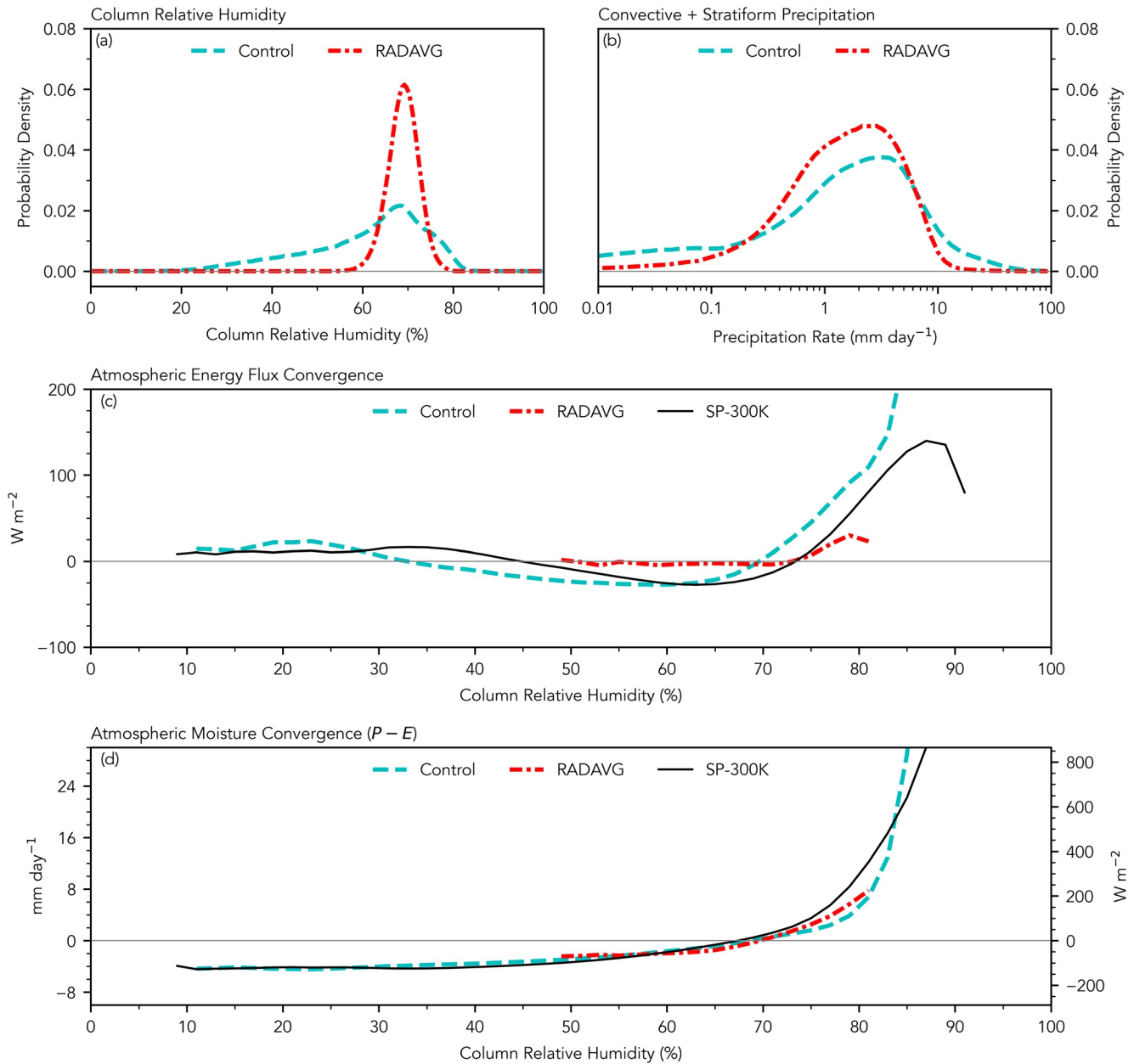
We took advantage of the relative efficiency of performing the calculations without SP to run both simulations for 10 months, although an equilibrium state was reached after about a month (not shown). These simulations also demonstrate that our main conclusions are replicated in a model without SP. The following analysis utilizes daily mean model output from a 30-day period near the end of each simulation.

Figure 9 shows snapshots of the CRH for an arbitrary time step to illustrate the differences between the Control and RadAvg simulations. The color bar is chosen to emphasize the rapid pickup in precipitation which occurs between 70% and 80% CRH (Bretherton et al., 2004). The control simulation contains extremely dry and extremely humid regions. In contrast, most regions of the RadAvg simulation range between 65% and 75% CRH.

To more quantitatively show the difference in humidity, panel (a) of Figure 10 shows the PDF of CRH for the Control and RadAvg simulations. The PDF for the RadAvg simulation is much taller and narrower, with a peak at 70% and tails that go to zero near 60% and 80%. The PDF for the Control simulation, in comparison, is much shorter and wider, and is similar to the PDFs shown in Figure 2 for the RCEMIP simulations. Due to the exponential dependence of precipitation on CRH, these distributions suggest that the RadAvg simulation should have fewer extreme precipitation events compared to the Control simulation. This is supported by panel (b) of Figure 10, which shows the PDF of the total precipitation rate on a logarithmic scale. The RadAvg and Control curves intersect near  $5 \text{ km day}^{-1}$ . As the precipitation rate increases above this value, the RadAvg PDF quickly decreases in magnitude, while the Control PDF has a much longer tail.

The effect of the narrow CRH distribution is illustrated in panels (c) and (d) of Figure 10, which show the atmospheric energy flux convergence and moisture convergence for the Control and RadAvg simulations, calculated identically to the curves in Figures 5 and 6. For the purpose of comparison, the corresponding curve for the 300 K RCEMIP simulation is also included.

The Control and RCEMIP curves in panel (c) are qualitatively similar, although the Control simulation curve is shifted to lower values of CRH. Both show a small amount of energy divergence in clear regions, and a much larger convergence in humid regions. Both curves also range from about 10% CRH to near 90%. In contrast, the RadAvg curve extends only between 50% and 80% CRH, as expected from panel (a). The RadAvg curve is near zero in clear regions, and is much smaller in magnitude in humid regions. This indicates that homogenized radiation leads to a reduction in atmospheric energy convergence, and implies a much smaller export of moist static energy from humid regions. The three moisture convergence curves (panel d) are essentially identical between 50% and 80% CRH.



**Figure 10.** (a) Probability density function of column relative humidity (CRH) for Control (light blue, dashed) and RadAvg (red, dash-dotted) simulations. Compare with Figure 2. (b) Same as (a), but for the total precipitation rate on a logarithmic scale. (c) Moisture convergence as a function of CRH for the Control and RadAvg simulations. The moisture convergence curve for the SP-300 K simulation (black, solid) is also included for comparison. (d) Same as (c), but for the atmospheric energy convergence.

This budget analysis suggests that radiation is directly involved in the export of energy from humid regions. Radiation does not appear to be directly involved in the convergence of moisture into humid regions because moisture convergence (via precipitation) is such a strong function of CRH. Instead, radiation appears to be indirectly involved by widening the distribution of CRH to allow the larger CRH values that are associated with intense moisture convergence.

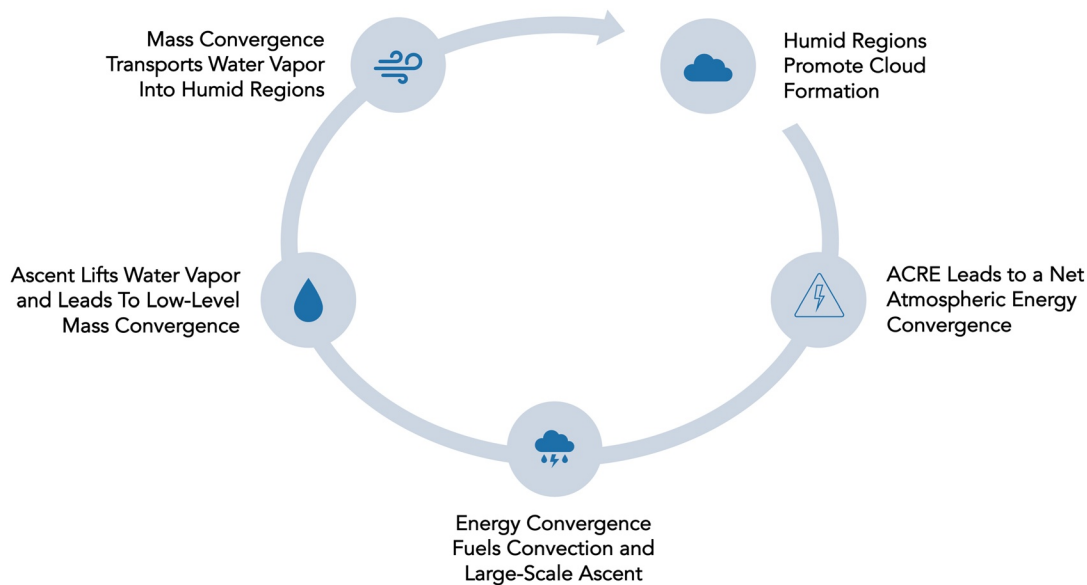


**Figure 11.** Diagram showing the cloud-longwave feedback described in the text. ACRE, atmospheric cloud radiative effect.

## 7. Conclusions

### 7.1. A Longwave-Cloud Feedback in the Tropics

Our results suggest that a cloud-longwave feedback is a fundamental characteristic of very humid regions of the tropics. First, clouds preferentially form in humid regions, where they absorb radiation, especially in the longwave. If the ACRE is large enough, it leads to a net radiative heating throughout the depth of the troposphere. This heating then drives environmental ascent which lifts water vapor and homogenizes the moist static energy, making convective-scale ascent unnecessary for vertical energy transport. The rising motion also drives low-level moisture convergence (Neelin & Held, 1987), which transports water vapor from dry regions into humid regions, against the moisture gradient, as in the ITCZ (Riehl & Malkus, 1958). This provides a steady source of moisture for regions that are already humid, which widens the CRH distribution, supports further cloud formation, and completes the feedback loop. The steps of this feedback are summarized in Figure 11.

### 7.2. Discussion

We have performed an energy and moisture budget analysis of a set of GCM simulations configured in radiative convective equilibrium over a nonrotating ocean with uniform fixed SSTs and insolation. Our results show that humid regions in these simulations export energy and import moisture in a way that is analogous to the ITCZ as first analyzed by Riehl and Malkus (1958), even though the simulations omit the rotation and temperature gradients necessary to form a true ITCZ. We then analyzed the vertical structure of moist static energy, and found that the characteristic mid-tropospheric minimum becomes weak in humid regions, likely due to environmental-scale ascent (Jenney et al., 2020), which tends to vertically homogenize  $h$ . Our analysis emphasizes the importance of the longwave ACRE in humid regions of the tropics. We find that the ACRE is strong enough to change the sign of the net radiation tendency in humid regions, and it is this heating which drives the environmental ascent.

Analysis of an additional simulation showed that homogenized radiative heating leads to a narrower distribution of CRH, with fewer extremely dry or humid regions than the control simulation. The atmospheric energy flux convergence in humid regions was also greatly reduced in this case, although moisture convergence as a function of CRH was largely unchanged.

Our analysis illustrates a general tropical cloud-longwave feedback that exists both in this extremely idealized modeling framework and in the real world. The feedback is similar to those that have been described

elsewhere in the literature in a variety of contexts (discussed in Section 1). Similar analysis performed on two sets of rotating aquaplanet experiments (one with super-parameterization, and one without) that include a meridional SST gradient and diurnal cycle yielded essentially identical results to those presented here (Needham, 2021).

Our study also supports the main conclusion of Needham and Randall (2021), namely that the ACRE depends on the CRH in a nonlinear way that is similar to the well-known behavior of precipitation, and that the ACRE as a function of the CRH is largely independent of the SST. This suggests that the longwave effect of tropical clouds is decoupled from the SST, consistent with the fixed anvil temperature hypothesis (Hartmann & Larson, 2002; Zelinka & Hartmann, 2010). The behavior of longwave CREs in a warmer climate may instead be governed by changes in humidity. The PDFs of CRH in Figure 2 show an increase in the probability of both extremely dry and extremely humid regions as the SST increases, with little change in the mean CRH (Table 1). The increased frequency of humid regions would suggest an increase in grid cells with a large ACRE, while the increased frequency of dry regions would suggest the opposite. These competing effects complicate drawing simple conclusions about the mean behavior of longwave CREs in a warmer climate, and may help to explain the non-monotonic relationship between SST and the TOA CRE as presented in Table 1. These possibilities are left for future work.

## Data Availability Statement

This study utilized model output used originally by Jenney et al. (2020), which is available online (<https://hdl.handle.net/10217/199724>) as part of the Mountain Scholar institutional repository managed by the Colorado State University. The simulations analyzed in Section 6 are available online at <https://doi.org/10.5281/zenodo.4903598>.

## Acknowledgments

The authors thank Mark Branson for help with the simulations analyzed in Section 6, as well as Brandon Wolding and two anonymous reviewers for comments that greatly improved this manuscript. The authors also thank Professor J. Hurrell and Professor X. Gao for reading M. Needham's M.S. thesis, which includes an earlier version of this study. Support was provided by the National Oceanic and Atmospheric Administration through grant number NA19OAR4590155, and by the National Science Foundation through grant number AGS-1826643, both to the Colorado State University.

## References

- Ahmed, F., & Schumacher, C. (2015). Convective and stratiform components of the precipitation-moisture relationship. *Geophysical Research Letters*, 42(23). <https://doi.org/10.1002/2015gl066957>
- Albern, N., Voigt, A., Buehler, S. A., & Grützun, V. (2018). Robust and nonrobust impacts of atmospheric Cloud-Radiative interactions on the tropical circulation and its response to surface warming. *Geophysical Research Letters*, 27, 4937–8585. <https://doi.org/10.1029/2018GL079599>
- Allan, R. P. (2011). Combining satellite data and models to estimate cloud radiative effect at the surface and in the atmosphere. *Meteorological Applications*, 18(3), 324–333. <https://doi.org/10.1002/met.285>
- Arnold, N. P., & Randall, D. A. (2015). Global-scale convective aggregation: Implications for the Madden-Julian oscillation: Global-scale convective aggregation. *Journal of Advances in Modeling Earth Systems*, 7(4), 1499–1518. <https://doi.org/10.1002/2015ms000498>
- Benedict, J. J., Medeiros, B., Clement, A. C., & Olson, J. G. (2020). Investigating the role of cloud-radiation interactions in subseasonal tropical disturbances. *Geophysical Research Letters*, 47(9), e2019GL086817. <https://doi.org/10.1029/2019gl086817>
- Bony, S., Dufresne, J.-L., Le Treut, H., Morcrette, J.-J., & Senior, C. (2004). On dynamic and thermodynamic components of cloud changes. *Climate Dynamics*, 22(2–3), 71–86. <https://doi.org/10.1007/s00382-003-0369-6>
- Bretherton, C. S., Blossey, P. N., & Khairoutdinov, M. (2005). An energy-balance analysis of deep convective self-aggregation above uniform SST. *Journal of the Atmospheric Sciences*, 62(12), 4273–4292. <https://doi.org/10.1175/jas3614.1>
- Bretherton, C. S., Peters, M. E., & Back, L. E. (2004). Relationships between water vapor path and precipitation over the tropical oceans. *Journal of Climate*, 17(7), 1517–1528. [https://doi.org/10.1175/1520-0442\(2004\)017<1517:rbwvpa>2.0.co;2](https://doi.org/10.1175/1520-0442(2004)017<1517:rbwvpa>2.0.co;2)
- Byrne, M. P., Pendergrass, A. G., Rapp, A. D., & Wodzicki, K. R. (2018). Response of the intertropical convergence zone to climate change: Location, width, and strength. *Current Climate Change Reports*, 4(4), 355–370. <https://doi.org/10.1007/s40641-018-0110-5>
- Charney, J. G. (1963). A note on large-scale motions in the tropics. *Journal of the Atmospheric Sciences*, 20(6), 607–609. [https://doi.org/10.1175/1520-0469\(1963\)020<0607:anolsm>2.0.co;2](https://doi.org/10.1175/1520-0469(1963)020<0607:anolsm>2.0.co;2)
- Chen, J., & Bordoni, S. (2014). Orographic effects of the Tibetan Plateau on the East Asian summer monsoon: An energetic perspective. *Journal of Climate*, 27(8), 3052–3072. <https://doi.org/10.1175/JCLI-D-13-00479.1>
- Chikira, M. (2014). Eastward-propagating intraseasonal oscillation represented by Chikira-Sugiyama cumulus parameterization. Part II: Understanding moisture variation under weak temperature gradient balance. *Journal of the Atmospheric Sciences*, 71(2), 615–639. <https://doi.org/10.1175/jas-d-13-038.1>
- Harrison, E. F., Minnis, P., Barkstrom, B. R., Ramanathan, V., & Gibson, G. G. (1990). Seasonal variation of cloud radiative forcing derived from the earth radiation budget experiment. *Journal of Geophysical Research*, 95(D11). <https://doi.org/10.1029/JD095iD11p18687>
- Harrop, B. E., & Hartmann, D. L. (2016). The role of cloud radiative heating in determining the location of the ITCZ in aquaplanet simulations. *Journal of Climate*, 29(8), 2741–2763. <https://doi.org/10.1175/JCLI-D-15-0521.1>
- Hartmann, D. L., & Berry, S. E. (2017). The balanced radiative effect of tropical anvil clouds: Balance anvil clouds. *Journal of Geophysical Research: Atmospheres*, 122(9), 5003–5020. <https://doi.org/10.1002/2017JD026460>
- Hartmann, D. L., & Larson, K. (2002). An important constraint on tropical cloud - Climate feedback. *Geophysical Research Letters*, 29(20), 12-1–12-4. <https://doi.org/10.1029/2002GL015835>
- Inoue, K., & Back, L. E. (2015). Gross moist stability assessment during TOGA COARE: Various interpretations of gross moist stability. *Journal of the Atmospheric Sciences*, 72(11), 4148–4166. <https://doi.org/10.1175/JAS-D-15-0092.1>

- Janiga, M. A., & Zhang, C. (2016). MJO moisture budget during DYNAMO in a cloud-resolving model. *Journal of the Atmospheric Sciences*, 73(6), 2257–2278. <https://doi.org/10.1175/JAS-D-14-0379.1>
- Jenney, A. M., Randall, D. A., & Branson, M. D. (2020). Understanding the response of tropical ascent to warming using an energy balance framework. *Journal of Advances in Modeling Earth Systems*. <https://doi.org/10.1029/2020ms002056>
- Khairoutdinov, M. F., & Emanuel, K. (2018). Intraseasonal variability in a cloud-permitting near-global equatorial aquaplanet model. *Journal of the Atmospheric Sciences*, 75(12), 4337–4355. <https://doi.org/10.1175/JAS-D-18-0152.1>
- Khairoutdinov, M. F., & Randall, D. A. (2003). Cloud resolving modeling of the ARM summer 1997 IOP: Model formulation, results, uncertainties, and sensitivities. *Journal of the Atmospheric Sciences*, 60(4), 607–625. [https://doi.org/10.1175/1520-0469\(2003\)060<0607:crmota>2.0.co;2](https://doi.org/10.1175/1520-0469(2003)060<0607:crmota>2.0.co;2)
- Li, Y., Thompson, D. W. J., & Bony, S. (2015). The influence of atmospheric cloud radiative effects on the large-scale atmospheric circulation. *Journal of Climate*, 28(18), 7263–7278. <https://doi.org/10.1175/JCLI-D-14-00825.1>
- Masunaga, H., & L'Ecuyer, T. S. (2014). A mechanism of tropical convection inferred from observed variability in the moist static energy budget. *Journal of the Atmospheric Sciences*, 71(10), 3747–3766. <https://doi.org/10.1175/JAS-D-14-0015.1>
- Medeiros, B., Clement, A. C., Benedict, J. J., & Zhang, B. (2021). Investigating the impact of cloud-radiative feedbacks on tropical precipitation extremes. *npj Climate and Atmospheric Science*, 4(1). <https://doi.org/10.1038/s41612-021-00174-x>
- Needham, M. R. (2021). *Links between atmospheric cloud radiative effects and tropical circulations* (Unpublished master's thesis). Colorado State University. <https://hdl.handle.net/10217/232508>
- Needham, M. R., & Randall, D. A. (2021). Linking atmospheric cloud radiative effects and tropical precipitation. *Geophysical Research Letters*, 48, e2021GL094004. <https://doi.org/10.1029/2021GL094004>
- Neelin, J. D., & Held, I. M. (1987). Modeling tropical convergence based on the moist static energy budget. *Monthly Weather Review*, 115(1), 3–12. [https://doi.org/10.1175/1520-0493\(1987\)115<0003:mtcbot>2.0.co;2](https://doi.org/10.1175/1520-0493(1987)115<0003:mtcbot>2.0.co;2)
- Neelin, J. D., Peters, O., & Hales, K. (2009). The transition to strong convection. *Journal of the Atmospheric Sciences*, 66(8), 2367–2384. <https://doi.org/10.1175/2009JAS2962.1>
- Peters, O., & Neelin, J. D. (2006). Critical phenomena in atmospheric precipitation. *Nature Physics*, 2(6), 393–396. <https://doi.org/10.1038/nphys314>
- Popp, M., & Silvers, L. G. (2017). Double and single ITCZs with and without clouds. *Journal of Climate*, 30(22), 9147–9166. <https://doi.org/10.1175/JCLI-D-17-0062.1>
- Powell, S. W. (2019). Observing possible thermodynamic controls on tropical marine rainfall in moist environments. *Journal of the Atmospheric Sciences*, 76(12), 3737–3751. <https://doi.org/10.1175/jas-d-19-0144.1>
- Ramanathan, V. (1987). The role of earth radiation budget studies in climate and general circulation research. *Journal of Geophysical Research*, 92(D4), 4075. <https://doi.org/10.1029/JD092iD04p04075>
- Ramanathan, V., Cess, R. D., Harrison, E. F., Minnis, P., Barkstrom, B. R., Ahmad, E., & Hartmann, D. (1989). Cloud-Radiative forcing and climate: Results from the earth radiation budget experiment. *Science*, 243(4887), 57–63. <https://doi.org/10.1126/science.243.4887.57>
- Randall, D. A., DeMott, C., Stan, C., Khairoutdinov, M., Benedict, J., McCrary, R., et al. (2016). Simulations of the tropical general circulation with a multiscale global model. *Meteorological Monographs*, 56, 15.1–15.15. <https://doi.org/10.1175/amsmonographs-d-15-0016.1>
- Randall, D. A., Harshvardhan, Dazlich, D. A., & Corsetti, T. G. (1989). Interactions among radiation, convection, and large-scale dynamics in a general circulation model. *Journal of the Atmospheric Sciences*, 46(13), 1943–1970. [https://doi.org/10.1175/1520-0469\(1989\)046<1943:iarcal>2.0.co;2](https://doi.org/10.1175/1520-0469(1989)046<1943:iarcal>2.0.co;2)
- Raymond, D. J. (2000). Thermodynamic control of tropical rainfall. *Quarterly Journal of the Royal Meteorological Society*, 126(564), 889–898. <https://doi.org/10.1002/qj.49712656406>
- Raymond, D. J., Sessions, S. L., Sobel, A. H., & Fuchs, Ž. (2009). The mechanics of gross moist stability. *Journal of Advances in Modeling Earth Systems*, 1(3). <https://doi.org/10.3894/JAMES.2009.1.9>
- Raymond, D. J., & Zeng, X. (2005). Modelling tropical atmospheric convection in the context of the weak temperature gradient approximation. *Quarterly Journal of the Royal Meteorological Society*, 131(608), 1301–1320. <https://doi.org/10.1256/qj.03.97>
- Riehl, H., & Malkus, J. S. (1958). On the heat balance in the equatorial trough zone. *Geophysica*, 6, 503–537.
- Ruppert, J. H., Wing, A. A., Tang, X., & Duran, E. L. (2020). The critical role of cloud-infrared radiation feedback in tropical cyclone development. *Proceedings of the National Academy of Sciences*, 117(45), 27884–27892. <https://doi.org/10.1073/pnas.2013584117>
- Rushley, S. S., Kim, D., Bretherton, C. S., & Ahn, M.-S. (2018). Re-examining the non-linear moisture-precipitation relationship over the tropical oceans. *Geophysical Research Letters*, 45(2), 1133–1140. <https://doi.org/10.1002/2017GL076296>
- Sherwood, S. C., Ramanathan, V., Barnett, T. P., Tyree, M. K., & Roeckner, E. (1994). Response of an atmospheric general circulation model to radiative forcing of tropical clouds. *Journal of Geophysical Research*, 99(D10), 20829. <https://doi.org/10.1029/94jd01632>
- Slingo, A., & Slingo, J. M. (1988). The response of a general circulation model to cloud longwave radiative forcing. I: Introduction and initial experiments. *Quarterly Journal of the Royal Meteorological Society*, 114(482), 1027–1062. <https://doi.org/10.1002/qj.49711448209>
- Sobel, A. H., Nilsson, J., & Polvani, L. M. (2001). The weak temperature gradient approximation and balanced tropical moisture waves. *Journal of the Atmospheric Sciences*, 58(23), 3650–3665. [https://doi.org/10.1175/1520-0469\(2001\)058<3650:twtgaa>2.0.co;2](https://doi.org/10.1175/1520-0469(2001)058<3650:twtgaa>2.0.co;2)
- Voigt, A., & Albern, N. (2019). No cookie for climate change. *Geophysical Research Letters*, 46(24), 14751–14761. <https://doi.org/10.1029/2019GL084987>
- Voigt, A., Albern, N., Ceppi, P., Grise, K., Li, Y., & Medeiros, B. (2021). Clouds, radiation, and atmospheric circulation in the present-day climate and under climate change. *Wiley Interdisciplinary Reviews: Climate Change*, 12(2). <https://doi.org/10.1002/wcc.694>
- Wing, A. A., Emanuel, K., Holloway, C. E., & Muller, C. (2017). Convective self-aggregation in numerical simulations: A review. *Surveys in Geophysics*, 38(6), 1173–1197. <https://doi.org/10.1007/s10712-017-9408-4>
- Wing, A. A., & Emanuel, K. A. (2014). Physical mechanisms controlling self-aggregation of convection in idealized numerical modeling simulations. *Journal of Advances in Modeling Earth Systems*, 6(1), 59–74. <https://doi.org/10.1002/2013ms000269>
- Wing, A. A., Reed, K. A., Satoh, M., Stevens, B., Bony, S., & Ohno, T. (2018). Radiative-convective equilibrium model intercomparison project. *Geoscientific Model Development*, 11(2), 793–813. <https://doi.org/10.5194/gmd-11-793-2018>
- Wing, A. A., Stauffer, C. L., Becker, T., Reed, K. A., Ahn, M., Arnold, N. P., et al. (2020). Clouds and convective self-aggregation in a multi-model ensemble of radiative-convective equilibrium simulations. *Journal of Advances in Modeling Earth Systems*. <https://doi.org/10.1029/2020MS002138>
- Wolding, B., Dias, J., Kiladis, G., Ahmed, F., Powell, S. W., Maloney, E., & Branson, M. (2020). Interactions between moisture and tropical convection. Part I: The coevolution of moisture and convection. *Journal of the Atmospheric Sciences*, 77(5), 1783–1799. <https://doi.org/10.1175/jas-d-19-0225.1>

- Wolding, B. O., & Maloney, E. D. (2015). Objective diagnostics and the Madden–Julian oscillation. Part II: Application to moist static energy and moisture budgets. *Journal of Climate*, 28(19), 7786–7808. <https://doi.org/10.1175/JCLI-D-14-00689.1>
- Wolding, B. O., Maloney, E. D., & Branson, M. (2016). Vertically resolved weak temperature gradient analysis of the Madden–Julian oscillation in SP-CESM. *Journal of Advances in Modeling Earth Systems*, 8(4), 1586–1619. <https://doi.org/10.1002/2016ms000724>
- Wolding, B. O., Maloney, E. D., Henderson, S., & Branson, M. (2017). Climate change and the Madden-Julian oscillation: A vertically resolved weak temperature gradient analysis. *Journal of Advances in Modeling Earth Systems*, 9(1), 307–331. <https://doi.org/10.1002/2016ms000843>
- Zelinka, M. D., & Hartmann, D. L. (2010). Why is longwave cloud feedback positive? *Journal of Geophysical Research*, 115(D16). <https://doi.org/10.1029/2010JD013817>